Materials Today Bio 6 (2020) 100046

Contents lists available at ScienceDirect

Materials Today Bio

journal homepage: www.journals.elsevier.com/materials-today-bio

Role of active nanoliposomes in the surface and bulk mechanical properties of hybrid hydrogels

R. Kadri [a,f], J. Bacharouch [a,f], K. Elkhoury [a], G. Ben Messaoud [a], C. Kahn [a], S. Desobry [a], M. Linder [a], A. Tamayol [b], G. Francius [c,d], J.F. Mano [e], L. Sánchez-González [a], E. Arab-Tehrany [a,*]

[a] Université de Lorraine, Laboratoire Ingénierie des Biomolécules, TSA 40602, Vandoeuvre-lès-Nancy, F-54518, France
[b] Department of Mechanical and Materials Engineering, University of Nebraska, Lincoln, NE, 68508, USA
[c] Université de Lorraine, Laboratoire de Chimie Physique et Microbiologie pour L'Environnement, UMR 7564, Villers-lès-Nancy, F-54601, France
[d] CNRS, Laboratoire de Chimie Physique et Microbiologie pour L'Environnement, UMR 7564, Villers-lès-Nancy, F-54601, France
[e] Department of Chemistry, CICECO - Aveiro Institute of Materials, University of Aveiro, 3810-193, Aveiro, Portugal

ARTICLE INFO

Keywords:
Liposomes
GelMA
Alginate
IPN hydrogels
Nanofunctionalization

ABSTRACT

Nanoliposomes are widely used as delivery vehicles for active compounds. Nanoliposomes from rapeseed phospholipids were incorporated into interpenetrating polymer network hydrogels of gelatin methacryloyl and alginate. The multiscale physicochemical properties of the hydrogels are studied both on the surface and through the thickness of the 3D network. The obtained composite hydrogels exhibited strong mechanical properties and a highly porous surface. The blend ratio, as well as the concentration of nanoliposomes, affects the properties of the hydrogels. Nanofunctionalized hydrogels induced keratinocyte growth. These advantageous characteristics may open up many applications of the developed hydrogels in drug delivery and tissue engineering.

1. Introduction

Hydrogels are three-dimensional (3D) networks of insoluble polymer matrices that can swell significantly while maintaining their structural integrity [1]. They have been extensively used in tissue engineering, as scaffolds supporting cell attachment, proliferation, growth, and differentiation, as well as in drug delivery systems [2–4]. Other biomedical applications of hydrogels include self-healing materials, biosensors, and hemostatic bandages [5]. Hydrogels resemble the native extracellular matrix, and they present inherent cellular interactions, excellent biological performance, good biocompatibility, and a high water content, which make them an ideal choice for tissue engineering applications [6]. Hydrogel porosity permits fluid flux and local angiogenesis which is crucial for oxygen, nutrient, and waste product diffusion [3,7]. However, their relatively weak mechanical properties limit their application as load-bearing tissue scaffolds. Several alternatives have been proposed to improve their mechanical properties [8,9], such as double-network hydrogels [10–12], nanocomposite hydrogels [13,14], and ionically cross-linked triblock copolymer hydrogels [15].

Hydrogels produced from natural biopolymers are widely used in the biomedical and pharmaceutical sectors [16–18]. Alginate and gelatin are two widely used biopolymers due to their excellent biodegradability and biocompatibility [17,19]. Alginate is a hydrophilic, biocompatible, and non-immunogenic polysaccharide that is mainly produced from brown algae [20]. Alginate-based hydrogels are widely used for tissue engineering applications because of their stability, ease of handling, and fast cross-linking process under mild conditions [21–23]. However, the small pore size distribution and lack of cell-binding moieties are key challenges facing alginate-based hydrogels. On the other hand, gelatin is a low-cost, translucent, soluble, and colorless protein acquired by partial hydrolysis of collagen. Gelatin is extracted mainly from mammalian sources, such as pig skin and bovine hides [24]. Gelatin promotes adhesion, spreading, and proliferation of various cell lines. To make photocrosslinkable hydrogels, gelatin methacryloyl (GelMA) is synthesized by the addition of methacryloyl groups to the gelatin backbone [22]. GelMA hydrogels possess natural cell-binding, degradation motifs, and their properties can be easily adjusted [25].

Nanoparticles (NPs) can be engineered from different sources (metals, minerals, semiconductors, and polymers) and into various shapes (tubes, wires, shells, rods, and spheres) [2,26–28]. These nanosized fillers can hugely affect the physical properties of the nanofunctionalized hydrogel, allowing for the engineering of enhanced biomaterials. NPs have a larger

* Corresponding author.
E-mail address: elmira.arab-tehrany@univ-lorraine.fr (E. Arab-Tehrany).
[f] Co-first author.

https://doi.org/10.1016/j.mtbio.2020.100046
Received 6 November 2019; Received in revised form 16 February 2020; Accepted 17 February 2020
Available online 27 February 2020

surface area than microsized fillers, which on a tight interface with polymeric matrices improves their mechanical properties. NPs help in maintaining the favorable biocompatibility of hydrogels, while also improving their biological properties, by influencing protein adsorption, as well as cell adhesion, proliferation, growth, and differentiation [29]. NPs are divided into hard (inorganic and metallic particles, quantum dots, and carbon nanotubes) and soft (liposomes, dendrimers, polymeric micelles, and nanogels) NPs [30,31]. Soft NPs are considered more biocompatible and biodegradable than hard inorganic NPs. Thus, for biomedical applications, especially for tissue engineering scaffolds, the use of soft organic NPs is preferable.

Here, we present synthesis and characterization of interpenetrating polymer network (IPN) hydrogels, produced from alginate and nano-functionalized polymerized GelMA, with soft nanoliposomes that contain essential natural micronutrients (omega-3 and omega-6) in their structure.

2. Materials and methods

2.1. Reagents

Phosphate-buffered saline (PBS) tablets, alginic acid sodium salt (M/G ratio = 1.56), calcium chloride ($CaCl_2$), methacrylic anhydride (MA), gelatin (type A), and 2-hydroxy-4'-(2-hydroxyethoxy)-2-methyl-propiophenone (photoinitiator[PI]) were purchased from Sigma-Aldrich (Chemie, Steinheim, Germany). Rapeseed lipids were extracted, without using organic solvents, via a low-temperature enzymatic process [32].

2.2. Characterization of rapeseed lecithin

Fatty acid methyl esters (FAMEs) were analyzed as previously described by Ackman [33]. In brief, FAME separation was carried out on a gas chromatography system equipped with a flame ionization detector, by using a fused silica capillary column. Both the detector and injector temperatures were fixed at 250 °C. Initially, the temperature of the fused silica capillary column was set at 120 °C for 3 min and increased later at a rate of 2 °C.min−1 to 180 °C, to be finally fixed at 220 °C for 25 min. Fatty acids were identified by comparison of the retention times with two complex qualitative standard mixtures PUFA No.1 and PUFA No.2 (Supelco, Sigma-Aldrich, Bellefonte, PA, USA). Measurements were carried out in triplicate.

2.3. Nanoliposome preparation

Rapeseed lecithin was dissolved in distilled water at a concentration of 3% and 5% (w/v). The suspension was mixed for 5 h under agitation in inert atmosphere (nitrogen) and then sonicated at a full power of 40% for 120 s (1 s on/1 s off) to get a homogeneous solution. Finally, the liposomal suspensions were stored in the dark at 37 °C until use.

2.4. GelMA preparation

Gelatin was dispersed at a concentration of 10 wt% in PBS at 60 °C and stirred until it was fully dissolved. Then, MA was added dropwise at a rate of 0.5 mL/min under stirring until the target volume was reached. After 3 h, the reaction was stopped with 5-fold dilution using warm PBS. Diluted GelMA was then dialyzed at 40–50 °C for one week using a dialysis membrane (MWCO 12–14,000). The solution was then lyophilized for one week. The freeze-dried GelMA foams were stored at −20 °C until further use.

2.5. Preparation of polymer solutions

To prepare alginate solution, 4 g of alginic acid sodium salt was dispersed into stirred 100 mL of double distilled water. After complete solubilization, the alginate solution was degassed to remove air bubbles. GelMA solution was prepared by dissolving the freeze-dried foam into a PBS solution at 40 °C. Then, 1% of the PI was added, and the temperature was increased to 80 °C to achieve complete solubilization. Both solutions were mixed at 40 °C to prepare alginate/GelMA solutions with final concentrations of 0.5, 1, 2, and 30 wt%.

2.6. Fabrication of discs

Alginate hydrogels were synthesized by carefully pouring 2 mL of 0.5, 1, and 2 wt% solutions in 5 mL of 2 wt% $CaCl_2$ solution in Petri dishes. GelMA solution was UV cross-linked (360–480 nm) in the specific mold for 240 s.

The fabrication of IPN hydrogels involved two separate steps. The first one consists of making a template by initial cross-linking of the mixture of the prepolymer and alginate using $CaCl_2$, which resulted in the formation of semi-IPN hydrogels. The second cross-linking step consists of UV illumination (360–480 nm) for 240 s for complete cross-linking of the prepolymer and formation of stable IPN discs.

2.7. Measurement of nanoliposome size and electrophoretic mobility

The size distribution (mean diameter and polydispersity index) and electrophoretic mobility (μE) of nanoliposome dispersions were measured by Malvern Zetasizer Nano ZS dynamic light scattering. The samples were diluted (1:400) with ultrapure distilled water. Measurements were completed in standard capillary electrophoresis cells equipped with gold electrodes at a scattering angle of 173°, a refractive index of 1.471, an absorbance of 0.01, and a temperature of 25 °C. Three independent measurements were made.

2.8. Scanning electron microscope low vacuum mode

Surface morphologies of hydrogels were characterized using a Quanta scanning electron microscope (FEI-Japan). The low-vacuum mode used allows the observation of surface topography of biomaterials without sputter coating while protecting them from electron beam damage. The maximal resolution attained could be lower than 5 nm, using an electron beam spot size of 7 nm. A large field detector (LFD) was used to execute this analysis. Square-shaped samples (9 mm × 9 mm) were inserted in the scanning electron microscope chamber, and tests were performed at a relative humidity of 50% and a temperature of 25 °C. Using partial vacuum, a regular pressure of 60 mbar was created. Images were taken from a 10-mm distance with an acceleration voltage of 15 kV and analyzed using 'xT microscope server' software.

2.9. X-ray photoelectron spectroscopy

X-ray photoelectron spectroscopy (XPS) were carried out using the KRATOS Axis Ultra X-ray photoelectron spectrometer and performed with monochromatic incident radiation Al–K α X-ray and a photon energy hv of 1486.6 eV. XPS is an effective technique to characterize the surface of the hydrogels and provide adequate information on the possible interactions in the hydrogel. The test was performed at 150 W and a base pressure of 10^{-9} mbar. Photoelectron data were recorded with survey scans at 1100-0 eV at an analyzer pass energy of 160 eV and narrow scans at an analyzer pass energy of 20 eV. The binding energies were corrected by setting the C_{1s} spectral to 284.6 eV.

2.10. Rheological measurements

A Malvern Kinexus rheometer equipped with a plate-and-plate geometry (20 mm) was used to measure the dynamic viscoelasticity. To determine the dynamic storage (G') and viscous (G") moduli, dynamic frequency sweep tests from 0.005 to 30 Hz were performed, at strain rates in the linear viscoelastic range. To minimize water evaporation, the measuring system was covered with a humidity chamber that was

maintained at 37 °C. Average values of three independent measurements are presented.

2.11. Measurements of elastic modulus by atomic force microscopy nanoindentation

The nanoindentation method provides Young's modulus values that are calculated from the force and indentation curve. Atomic force microscopy (AFM)measurements were conducted using an MFP3D-BIO instrument (Atomic Force F&E GmbH, Mannheim, Germany). SiO_2 triangular cantilevers with a colloidal probe (10-μm radius) were purchased from Novascan Inc. (Iowa State University Research Park, IA 50010, USA). Using the thermal noise method, spring constants of cantilevers were found to be 10 pN/nm. Experiments were performed in PBS at pH 7.4 and a temperature of 37 °C. Maps of mechanical properties (force volume image [FVI]) were obtained by recording a grid map of 32-by-32 force curves at 3

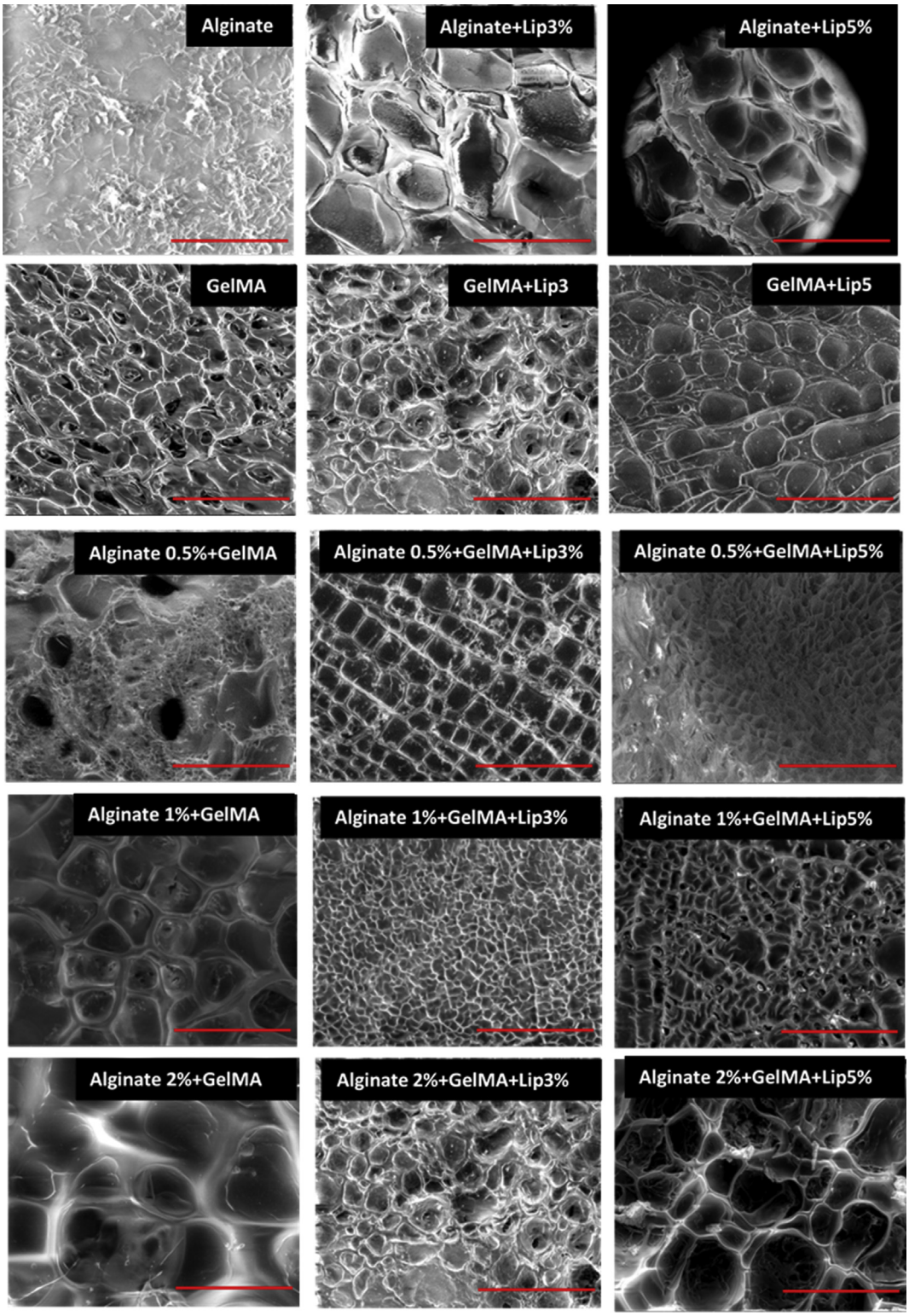

Fig. 1. SEM images of 3D hydrogels of various systems before and after functionalization. (Scale bar = 300 μm). 3D = three-dimensional; SEM = scanning electron microscopy; GelMA = gelatin methacryloyl.S= μ

different locations of the film surface (Fig. 2b). The maximal loading force was 6 nN. Elasticity maps and the corresponding histograms (statistic distribution) were estimated from the analysis of the approach curves as per the model used by Dimitriadis et al [34]:

$$F = \frac{4E}{3(1-\nu^2)} R^{1/2}\delta^{3/2}\left[1 + 1,133\chi + 1,283\chi^2 + 0,769\chi^3 - 0,0975\chi^4\right] \quad (1)$$

where δ is the indentation depth, ν is the Poisson coefficient, and R is the colloid radius. The Dimitriadis correction for finite thickness is defined by the χ parameter:

$$\chi = \frac{\sqrt{R\delta}}{h} \quad (2)$$

where h is the sample thickness. The FVI or force maps were analyzed by means of an automatic Matlab algorithm, described by Polyakov et al [35].

2.12. Scratch assay

Keratinocytes were cultured in a 24-well plate until a confluent cell layer was formed. Then, a 100-μm-wide scratch was formed using a P200 pipette tip, and the hydrogels with and without nanoliposomes were placed inside culture inserts (a pore size of 8 μm). Microscopic images were taken over a period of 24 h to identify the migration rate of keratinocytes and analyzed using Image J software. The coverage percentage was evaluated by measuring the scratch surface directly after scratching and after 24 h.

2.13. Metabolic activity

Keratinocytes were cultured at the bottom of a 96-well plate (an initial seeding density of 8000 cells per well), and then, 100 μL of alginate/GelMA hydrogels with and without nanoliposomes were placed inside the well plate. The metabolic activity of the cells was measured by PrestoBlue® assay (Life Technologies, Carlsbad, CA, USA). PrestoBlue® assay was performed as per the manufacturer's recommended protocol. One hundred fifty microliters of PrestoBlue®/culture media (1/10 v/v) was added into each well and incubated at 37 °C for 1 h. Afterward, 100μL of this medium was transferred into a new 96-well plate, and the solution's fluorescence was recorded at 560 nm (excitation) and 590 nm (emission) using a microplate reader (BioTek synergy™ 2, USA). Relative cell viability (R) was calculated as follows:

$$R\% = \frac{A_{test}}{A_{control}} \times 100 \quad (3)$$

where A_{test} and $A_{control}$ are the absorbance values of solutions collected from the cells that were treated with the test solutions and the blank culture medium, respectively.

3. Results and discussion

3.1. Liposome properties and chemical composition

The average nanoliposome size produced from rapeseed phospholipids was 110 nm, with an electrophoretic mobility of −3.41 μE. Based on FAME analysis by gas chromatography, the largest amount of fatty acid found in rapeseed phospholipids was the monounsaturated oleic acid C18:1 n-9 (57.80%). The major polyunsaturated fatty acids linoleic acid C18:2 n-6 and linolenic acid C18:3 n-3 comprised 26.32% and 6.60% of the rapeseed phospholipids, respectively. High concentrations of monounsaturated fats, such as oleic acid, combined with low concentrations of saturated fats, such as stearic and palmitic acids, have been shown to reduce the undesirable low-density lipoproteins without

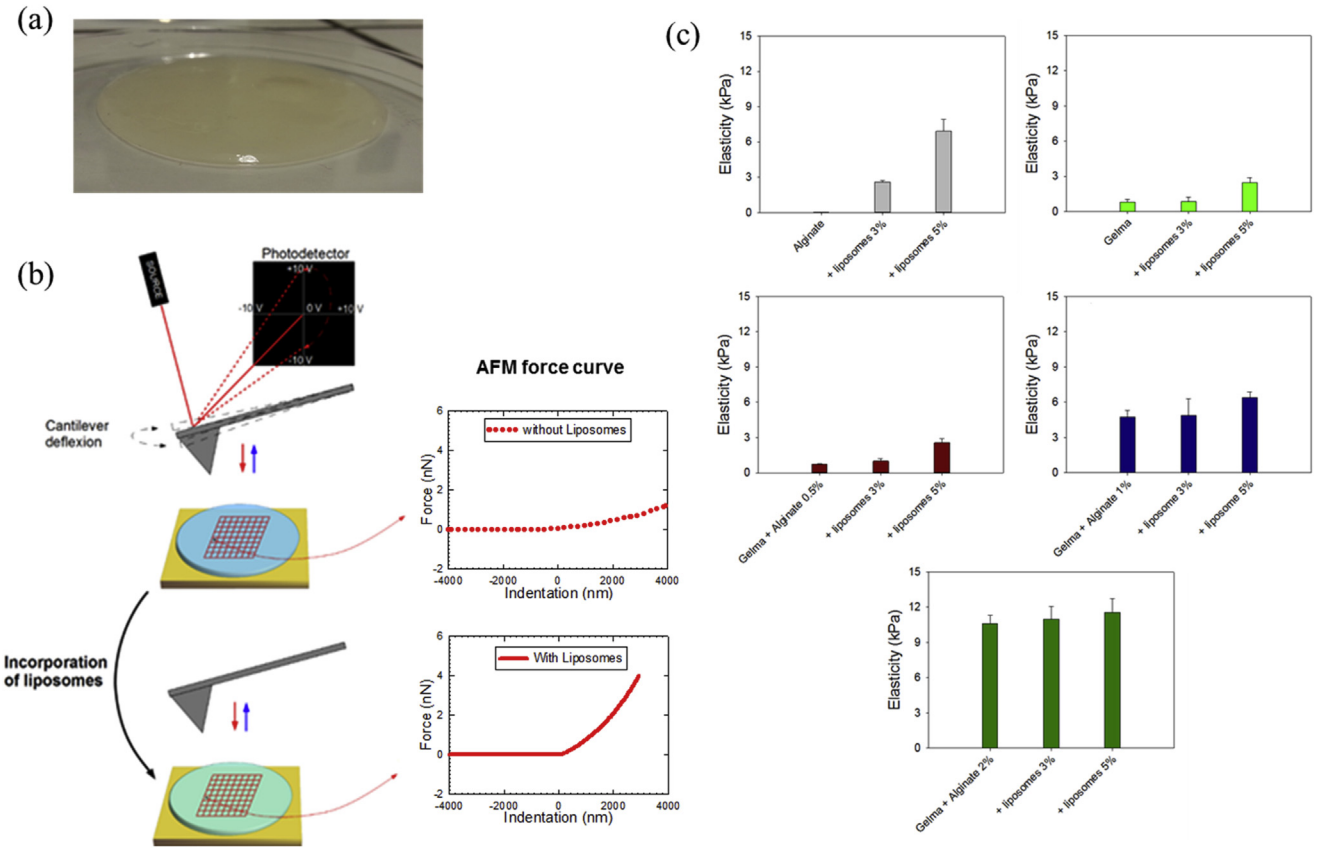

Fig. 2. (a) Image of the 3D structure of the hydrogel. (b) Typical AFM force curves. (c) Evolution of the elastic modulus of biomaterials before and after nanoliposome functionalization. 3D = three-dimensional; AFM = atomic force microscopy; GelMA = gelatin methacryloyl.

affecting the level of desirable high-density lipoproteins in human blood serum [36]. Moreover, although linoleic and linolenic acids cannot be synthesized by humans, they are considered essential fatty acids because they are important to human health [37]. The monounsaturated and polyunsaturated fatty acid composition of nanoliposomes provides a bioactive character to the soft NPs.

3.2. Surface properties of hydrogels

Freestanding nanoliposomes-IPN hydrogels (alginate and GelMA) with two nanoliposome concentrations were developed using sonication-free nanoliposomes and hydrogel formation by UV cross-linking of GelMA and $CaCl_2$ reticulation of alginate under appropriate physiological conditions.

3.2.1. Microstructure

The surface morphology of alginate, GelMA, and IPN alginate/GelMA discs before and after nanoliposome functionalization was studied to evaluate pore distribution and their architecture by scanning electron microscopy (SEM) (Fig. 1). The alginate disc displayed a folded surface structure in regular patterns. After adding the nanoliposomes into alginate, the disc surface at two concentrations of nanoliposomes showed a totally homogeneous surface morphology without any regular patterns of folding with regular pores. However, the disc of GelMA showed the porous nature of scaffold with a pore size ranging from 23 to 104 μm after nanofunctionalization. The nanoliposome nanofunctionalization of the alginate/GelMA matrix yielded heterogeneous and well-defined pores, as well as a highly interconnected porosity (Fig. 1). The interconnected porosity suits the scaffolds for cell attachment, migration into the deeper struts, and neovascularization [38,39]. The SEM results demonstrated that nanoliposomes modified the surface properties of hydrogels, in particular, the surface properties of alginate discs.

The incorporated nanoliposomes were non-fusogenic (the nanoliposomes were stable for more than 2 months); however, calcium cations could initiate their aggregation, and the close contacts between them might, therefore, facilitate lipid exchange and even fusion of lipid bilayers [40]. The presence of nanoliposomes, especially large-sized fused nanoliposomes, could form a spatial obstacle during cross-linking, which increases the resulting porosity of the cross-linked hydrogels (Fig. 1) [41].

3.2.2. Chemical structure and potential interactions

XPS, based on the distribution of electron energy, provides information about the surface composition of a material and characterizes possible interactions between the hydrogel components. Table 1 characterizes the surface of the different hydrogels.

The XPS analysis on the alginate hydrogel shows characteristic peaks of Na_{1s} at 1071.55 eV and O_{1s} at 532.45 eV. The C peak can be fitted to three components C-(C,H), C–O, and O–C=O. These elements are generated from the alginate polymer. The addition of $CaCl_2$ during the cross-linking and the formation of the alginate hydrogel are confirmed by the presence of Ca_{2p} and Cl_{2p} peaks at 347.25 eV and 198.55 eV, respectively. The incorporation of nanoliposomes into the alginate hydrogel showed similar peaks as the spectrum of alginate, but the atomic concentration percentage of the carbon increases from 54.63% to 78.11%. However, a new peak characteristic of the liposomes appeared at 133.06 eV, representing P_{2P}. The spectrum of alginate with liposomes did not present any new elements and did not show any interaction between the polymer and the NPs. Although the atomic concentration of calcium decreased to 50% with the addition of nanoliposomes, in fact, the changes seen on the spectrum may be due to an interaction between the soft NPs and the chelating agent Ca^{2+}, which had an impact on the cross-linking of alginate and calcium.

The spectrum of GelMA represented three essential components of the polymer: O_{1s} (531.150 eV), N_{1s} (399.650), and C_{1s} (284.650 eV). The N:C ratio was low, confirming the methacrylation of GelMA and the partial replacement of the amine groups by methacrylamide groups. The addition of nanoliposomes showed also the same elements as the GelMA spectrum. The nitrogen concentration decreased by 63% after the incorporation of the soft NPs. The P_{2P} peak of the liposomes appeared with a lower concentration than the alginate polymer. It is possible that the phosphate groups of liposomes have reacted with the amine groups of GelMA.

The IPN hydrogels containing 2% of alginate showed a new peak representing $C–NH^{3+}$, confirming the interaction between two polymers alginate and GelMA. After the addition of nanoliposomes, the phosphorus element appeared, evidencing the presence of liposomes in the solutions. It is remarkable that when alginate concentration was decreased, the nitrogen element, as well as phosphorus, disappeared. The obtained result highlights that the alginate concentration affected the interaction between the different components, leading to hydrogels with different properties. In fact, alginate and liposomes competed to react electrostatically with GelMA. The incorporation of nanoliposomes occurred after the mixture of the two polymers. Because alginate reacted first with GelMA, a decrease in the alginate concentration can increase the possibility for liposomes to interact with the free positive charges of GelMA.

3.3. Surface mechanical properties

Nanomechanical properties of the developed hydrogels were measured by AFM nanoindentation technique using a colloidal probe (Fig. 2b). Each bar and the corresponding errors were derived from an average of 1024 values (Fig. 2c). The statistic distribution of elastic modulus of each type of hydrogel and the force curves are given in the supplementary information section (Figs. S1–S5).

Hydrogels were based on pure gels from alginate or GelMA and also a mixture of GelMA and alginate at a ratio of 50:50 with various alginate

Table 1
XPS analysis of the surface elemental composition of pure alginate and GelMA IPN hydrogels, before and after functionalization with nanoliposomes.

Hydrogel	% O 1s	% C 1s	% N 1s	% O 1s O=C	% O 1s O–C	% N 1s C-(NH,NH2)	% C 1s C-(C,H)	% C 1s C–O	% C 1s C = O	% P 2p
Alg 2%	26.35	54.63	1.49	58.8	33.33	100	37.24	38.46	24.3	–
Alg 2% + lip 5%	17.47	78.11	–	27.96	65.83	–	68.44	22.85	4.47	0.62
GelMA	17.39	68.05	14.41	61.56	27.46	100	44.29	32.65	19.69	–
GelMA + lip 5%	16.21	74.33	9.09	49.64	35.61	100	55.01	27.87	13.05	0.38
Alg 2% + G	19.18	65.87	14.95	64.57	25.93	95.05	39.22	34.5	21.98	–
Alg 2% + G + lip 5%	17.48	72.40	9.24	47.41	38.71	93.97	53.40	28.22	13.97	0.3
Alg 1% + G	17.88	61.06	16.66	67.87	23.67	95.24	39.83	35.98	20.20	–
Alg 1% + G + lip 5%	20.86	77.8	–	44.28	44.48	–	55.20	27.76	12.34	0.51
Alg 0.5% + G	20.98	78.24	–	66.09	24.57	–	42.28	33.99	19.86	–
Alg 0.5% + G + lip 5%	20.76	78.77	–	59.21	29.10	–	43.60	30.87	20.84	–

XPS = X-ray photoelectron spectroscopy; GelMA = gelatin methacryloyl; IPN = interpenetrating polymer network.

concentrations of 0.5, 1, and 2 wt%. In addition, nanoliposomes were incorporated in the IPN hydrogels with two blending amounts of 3 and 5 wt%, respectively. Then, gels were analyzed by colloidal probe AFM, wherein 1024 measurements were taken over 20 × 20 μm^2 surface area for each sample and each replicate (Table 2).

The native and pure gels containing only alginate and GelMA are characterized by elastic moduli of about 0.05 ± 0.01 kPa and 0.81 ± 0.25 kPa, respectively. This result indicates that a 2 wt% alginate cross-linked hydrogel is 16 times softer than the GelMA samples. When the alginate hydrogel was blended with nanoliposomes at a concentration of 3 and 5 wt%, a drastic increase in the elastic modulus was observed. The elastic modulus increased from 0.05 kPa to 2.60 kPa and 6.97 kPa for the blending of 3 and 5% nanoliposomes, respectively (Table 2). This increase emphasized that the nanoliposomes are involved in the gel reinforcement with stiffening factors of ca. 50 and 140, respectively. In the case of the pure GelMA hydrogel, this effect is weaker with stiffening factors ranging only from 1 to 3. Mechanical property analysis of the mixed gel containing GelMA and alginate cross-linked at a concentration of 0.5% shows the same trend (i.e., a weak increase in the elastic modulus in the range of only 1 to 4). When the alginate concentration was increased, an increase in Young's modulus was observed from 0.74 kPa to 4.73 kPa and to 10.61 kPa for alginate concentrations of 0.5%, 1%, and 2%, respectively. Here, the stiffening effect seems to be driven by the alginate amount with stiffening rates of about 6 and 14 for 1% and 2% alginate, respectively. Surprisingly, the blending of 3 and 5 wt% of nanoliposomes leads to a slight increase of the elastic modulus of the mixed gels, with stiffening rates ranging from 1.05 to 1.42 and from 1.03 to 1.09 for the 1% and 2% cross-linked gels, respectively. This result underlines that the stiffer the mixed gel, the smaller the effect of nanoliposomes on the gel's mechanical properties.

3.4. Bulk mechanical properties

The mechanical properties along with the thickness of hydrogels were investigated by dynamic shear oscillation measurements. Influence of nanoliposomes on the viscoelastic properties of hydrogels at 37 °C at a mesoscopic scale was also studied. Typical mechanical spectra are shown in Fig. 3, in which average G′ and G″ are presented over a range of 0.05–30 Hz. Storage (or elastic) modulus represents the elastic part, and the loss (or viscous) modulus represents the viscous part of a material. All mechanical spectra showed that G′ is higher than G″, confirming that all hydrogels (alginate, GelMA, and IPN materials) have principally an elastic rather than a viscous character, which is what normally differentiates gels from viscous liquids and demonstrates that deformation energy is recovered in the elastic stretching of chemical bonds [42].

The slow increase of alginate hydrogel storage modulus with frequency (Fig. 3a) indicated the existence of relaxation processes that could be induced by the reversible release of the entrapped entanglements or by intermolecular junction opening [43]. These junctions resulted from the coordination of Ca^{2+} cations to the alginate's interchain cavities made up of G and MG blocks, resulting in the development of a so-called 'egg-box' [44]. The incorporation of nanoliposomes decreased significantly the storage modulus of alginate hydrogels. Most probably, the presence of nanoliposomes could affect the activity of Ca^{2+} during alginate gelation at room temperature, wherein nanoliposomes integrates into the gel state, which enhances the binding of Ca^{2+} owing to potential electrostatic interaction between the divalent cations and the negatively charged phospholipids [45]. The evolution of the elastic modulus of nanofunctionalized alginate hydrogels is in good agreement with their microstructure investigated by SEM and is presented in Fig. 1.

The storage modulus of all GelMA hydrogels was higher than the loss modulus (Fig. 3b), which proved that they were of an elastic nature at 37 °C. G' was notably constant throughout the increasing frequency range. Generally, mechanical stability of GelMA hydrogels results from both physical structuring and chemical cross-linking [46]. Physical gelation results from a triple helix thermoreversible conformation change into individual polypeptide coils at temperatures higher than ca. 40 °C. When cooled at temperatures lower than 35 °C, helix structures are formed from the association of the random coils joined locally, which then grow, interconnect, and form larger domains until the entire volume is percolated [47]. Chemical cross-linking results through photopolymerization of vinyl groups initiated through UV light, wherein it maintains the structure of the hydrogel via the C–C bond between GelMA macromolecules at 37 °C[46]. Nanoliposome incorporation decreased the elastic modulus, but not significantly, of GelMA hydrogels, which could be due to the soft nature of the nanoliposome membrane [43,44].

The Alg 2%-GelMA IPN hydrogel's mechanical spectrum (Fig. 3c) had the highest G′ and G″ without any significant frequency dependence. IPN gel's G′ is higher than that of GelMA and alginate hydrogels. Gelatin is composed of 18 non-uniformly distributed amino acids with both positive and negative charges, and its cationic property is basically due to lysine and arginine residues [48]. Therefore, the reinforcement role of nanoliposomes could be attributed to intermolecular forces through electrostatic interaction between the unmodified protonated GelMA amino groups and the negatively charged alginate. However, nanoliposome incorporation results in a significant decrease in the G′ and G″, which might be related to the preparation method of the IPN hydrogels. Semi-IPN hydrogel preparation, by alginate gelation with $CaCl_2$, is the first step of the IPN gelation procedure, which is then followed by GelMA cross-linking via UV exposure. Considering that the cross-linked alginate provides the majority of the mechanical stability of the IPN hydrogels, the incorporation of nanoliposomes interferes with the 'egg-box' formation and therefore decreases the elastic modulus of the IPN hydrogels. In contrast, for IPN hydrogels prepared with 1 and 0.5 wt% alginate (Fig. 3d and e), the incorporation of nanoliposomes did not affect the mechanical stability of the final 3D structures. In fact, the decrease of alginate polymer amounts could lead to higher chain mobility and therefore easier macromolecular arrangement, which will reduce the spatial hindrance effect of the incorporated nanoliposomes. On the other hand, at lower alginate concentrations (1 and 0.5 wt%), the final mechanical stiffness of the IPN gels is defined by cross-linked GelMA. As nanoliposome incorporation did not affect the pure GelMA hydrogels, the inclusion of nanoliposomes would not affect the mechanical stability of the IPN hydrogels.

From the rheological investigation of the different hydrogel systems, we can conclude that the 2% alginate-GelMA IPN hydrogel showed the highest mechanical stability. The variation of alginate concentration highlighted the major role of alginate in the preservation of the mechanical stability of the final IPN structure. The nanoliposome nanofunctionalization influence was closely related to the matrix composition and to the gelation procedure. In fact, the addition of Ca^{2+} during alginate gelation may accentuate its contribution to the final matrix stability owing to size increase derived from nanoliposome fusion and aggregation.

Table 2
Young's modulus of simple and composite hydrogels before and after nanofunctionalization.

Young modulus (kPa, n = 1024)				
Gel composition		Nanoliposome blending (%)		
Alginate	GelMA	0	3	5
0.5%	–	0.05 ± 0.01	2.60 ± 0.13	6.93 ± 0.98
–	+	0.81 ± 0.25	0.85 ± 0.37	2.45 ± 0.44
0.5%	+	0.74 ± 0.05	0.79 ± 0.05	2.58 ± 0.31
1%	+	4.73 ± 0.58	4.90 ± 1.00	6.70 ± 0.45
2%	+	10.61 ± 0.72	10.97 ± 1.10	11.57 ± 1.16

GelMA = gelatin methacryloyl.

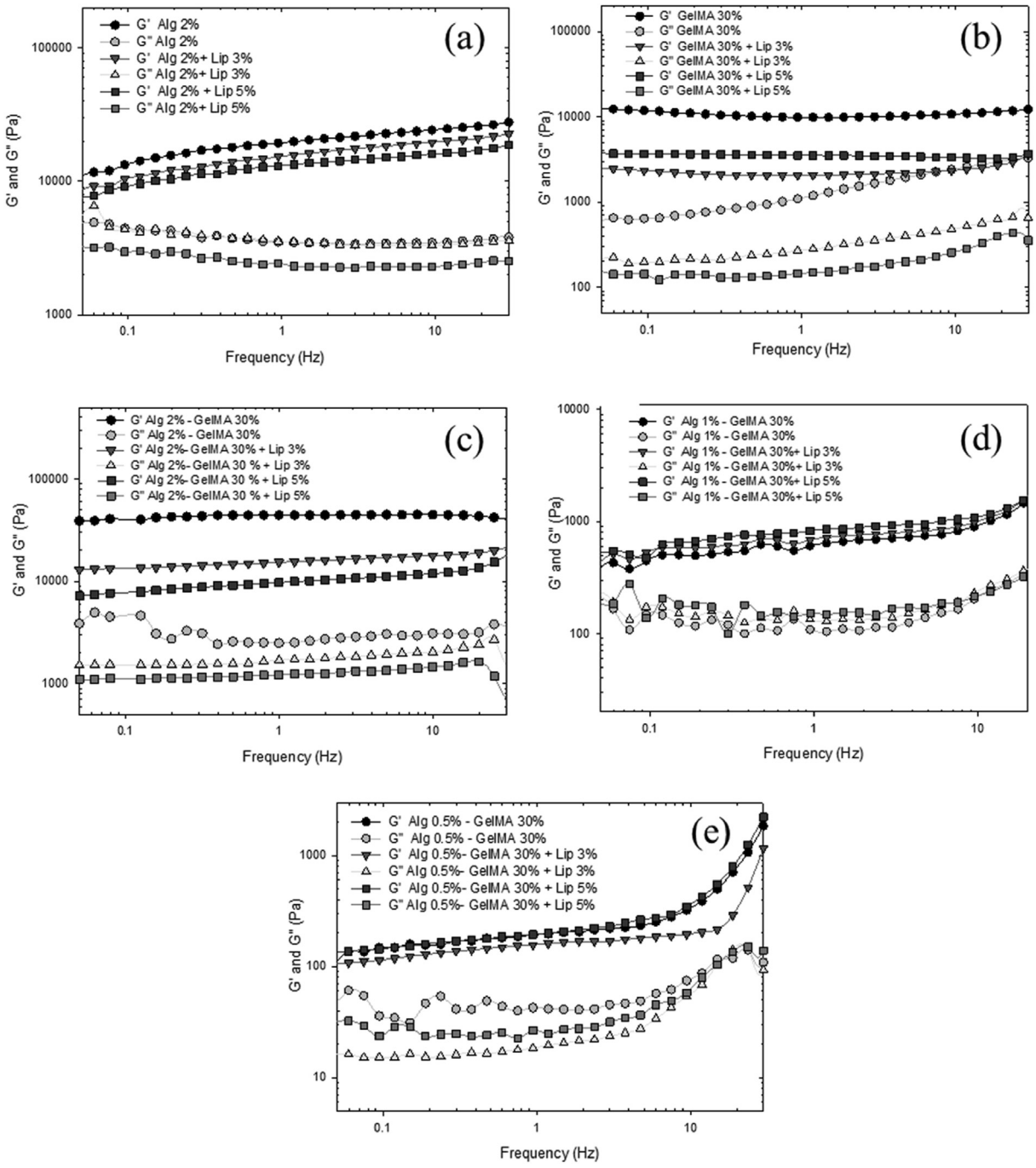

Fig. 3. Rheological properties of various hydrogels with and without nanoliposomes. Frequency sweep tests of (a) Alg 2%, (b) GelMa, (c) IPN of Alg 2% and GelMa 30%, (d) IPN of Alg 1% and GelMa 30%, and (e) IPN of Alg 0.5% and GelMa 30%. GelMa = gelatin methacryloyl; IPN = interpenetrating polymer network.

3.5. Biological properties

The designed hydrogel can be potentially used as a topical drug delivery system for wound healing applications. To assess the biological activity of the engineered hydrogel with and without nanoliposomes, we studied its interaction with human keratinocytes. A standard scratch assay was carried out to assess the nanoliposome effectiveness in inducing keratinocyte growth. First, ~500-μm-wide scratches were made over a confluent monolayer of keratinocytes. Next, pure and nanofunctionalized IPN hydrogels were placed inside culture inserts (a pore size of 8 μm) and incubated with cells for 24 h.

Keratinocyte migration was quantified by taking microscopy images from the cells at different time points. To obtain a scratch geometry–independent parameter for migration, the coverage percentage was calculated as follows:

$$\%\ \ coverage = \left(\frac{S_0 - S_t}{S_0}\right) \times 100$$

where S_0 is the scratch surface at time 0 and S_t is the scratched surface at time t. Fig. 4a shows microscopy images obtained at 0 h and 24 h after scratching a monolayer of keratinocytes. The coverage percentage at 24 h is calculated and shown in Fig. 4b. The results show that a significant increase in coverage percentage is achieved by incubating cells with nanofunctionalized hydrogels. The metabolic activity of cells directly cultured on pure and nanofunctionalized hydrogels was also studied

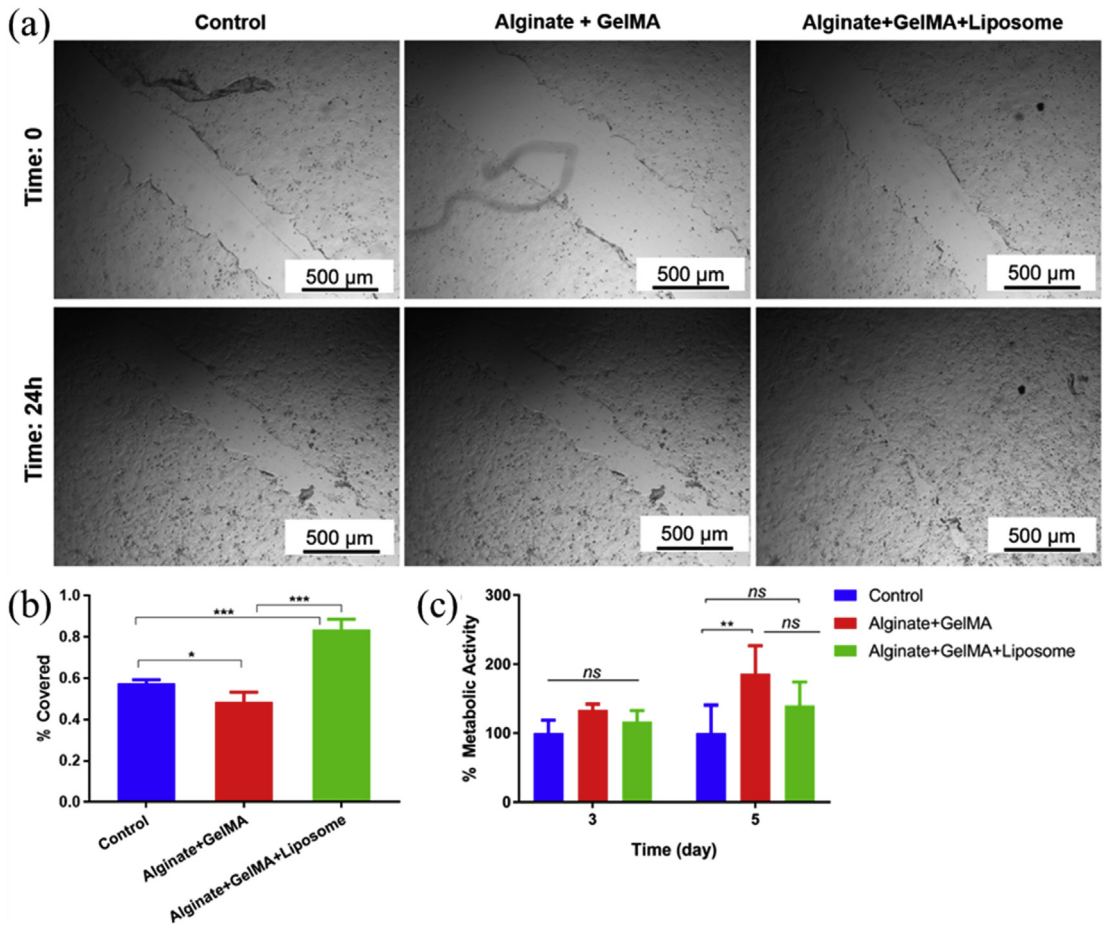

Fig. 4. The effect of nanoliposomes on the culture of keratinocytes. (a and b) A standard scratch assay was carried out in which ~500-µm-wide scratches were made and a treatment was applied to the scratched culture. The closed area of the scratch was measured after 24 h (a). (c) The metabolic activity of cells cultured directly at the interface of composite hydrogels with and without nanoliposomes was measured after 3 and 5 days of culture. The results showed that cells have remained viable during this period. GelMA = gelatin methacryloyl.

using a PrestoBlue viability assay. For this, 100 µL of hydrogel constructs with and without nanoliposomes was interfaced with freshly seeded cellular cultures. Fig. 4c shows the metabolic activity of cells after 3 and 5 days of incubation on IPN hydrogels. The results show that cells have retained their metabolic activity.

4. Conclusions

In summary, a robust approach for the fabrication of nano-functionalized 3D structures from IPN hydrogels was proposed. The inclusion of soft NPs (nanoliposomes) differently affected the mechanical properties of hydrogels at the surface and through the thickness. At the nanoscale, the elastic modulus investigated at the extreme surface increased significantly after nanoliposome inclusion for all hydrogel systems. However, at a larger scale, bulk rheology demonstrated that elastic modulus of hydrogels decreased on nanofunctionalization. In fact, the nanoliposome addition could influence the mechanical properties of the final matrix at two different stages: during the gelation process or after hydrogel formation. During the gelation process, nanoliposomes could form spatial obstacles and decrease the bulk roughness of hydrogels, whereas after hydrogel formation, the dynamic matrices may evolve and nanoliposomes could be pushed toward the surface owing to their low density and high mobility in the final material.

On the other hand, the nanofunctionalization of the alginate/GelMA IPN matrix with nanoliposomes resulted in modified surface properties. In addition, we confirmed that the presence of alginate can increase the mechanical properties of the engineered protein-based hydrogels. Nanoliposome functionalization of IPN hydrogels enhanced the growth of keratinocytes and thus improved the biological properties of these hydrogels.

Author contributions

The manuscript was written with the contributions of all authors. All authors have given approval to the final version of the manuscript. Conceptualization, validation, formal analysis: E.A.T., A.T., L.S.G., G.F.; investigation: R.K., J.B., K.E., G.B.M.., methodology: E.A.T., C.K., S.D., M.L., writing, review and editing: R.K., J.B., K.E., G.B.M., A.T., J.M.; supervision: EAT., L.S.G., G.F.

Declaration of competing interest

The authors declare that they have no known competing financial interests or personal relationships that could have appeared to influence the work reported in this paper.

Acknowledgments

R.K. and J.B. contributed equally to this work. The authors are grateful to the European Commission for the Erasmus Mundus grant to R.K. (Erasmus Mundus External Window 'ELEMENT' Program). The ANRT French agency (project No 312/2012) is also acknowledged for financial support to G.B.M. K.E. acknowledges support from the French Ministry of Higher Education, Research and Innovation. J.M.

acknowledges that this work was also developed within the scope of the funded project MARGEL (POCI-01-0145-FEDER-031498) and project CICECO-Aveiro Institute of Materials (POCI-01-0145-FEDER-007679 with Ref. FCT UID/CTM/50011/2013), financed by national funds through the FCT / MEC and, when appropriate, cofinanced by under the Partnership Agreement.

Appendix A. Supplementary data

Supplementary data to this article can be found online at https://doi.org/10.1016/j.mtbio.2020.100046.

References

[1] B.V. Slaughter, S.S. Khurshid, O.Z. Fisher, A. Khademhosseini, N.A. Peppas, Hydrogels in egenerative medicine, Adv. Mater. 21 (2009) 3307–3329, https://doi.org/10.1002/adma.200802106.
[2] K. Elkhoury, C.S. Russell, L. Sanchez Gonzalez, A. Mostafavi, T.J. Williams, C. Kahn, N.A. Peppas, E. Arab-Tehrany, A. Tamayol, Soft nanoparticle functionalization of natural hydrogels for tissue engineering applications, Adv. Healthcare Mater (2019) 1900506, https://doi.org/10.1002/adhm.201900506.
[3] N.A. Peppas, J.Z. Hilt, A. Khademhosseini, R. Langer, Hydrogels in biology and medicine: from molecular principles to bionanotechnology, Adv. Mater. 18 (2006) 1345–1360, https://doi.org/10.1002/adma.200501612.
[4] J.S. Boateng, K.H. Matthews, H.N.E. Stevens, G.M. Eccleston, Wound healing dressings and drug delivery systems: a review, J. Pharm. Sci. 97 (2008) 2892–2923, https://doi.org/10.1002/jps.21210.
[5] Q. Chai, Y. Jiao, X. Yu, Hydrogels for biomedical applications: their characteristics and the mechanisms behind them, Gels 3 (2017) 6, https://doi.org/10.3390/gels3010006.
[6] J.L. Drury, D.J. Mooney, Hydrogels for tissue engineering: scaffold design variables and applications, Biomaterials 24 (2003) 4337–4351.
[7] W. Xiao, J. He, J.W. Nichol, L. Wang, C.B. Hutson, B. Wang, Y. Du, H. Fan, A. Khademhosseini, Synthesis and characterization of photocrosslinkable gelatin and silk fibroin interpenetrating polymer network hydrogels, Acta Biomater. 7 (2011) 2384–2393, https://doi.org/10.1016/j.actbio.2011.01.016.
[8] A.M. Costa, J.F. Mano, Extremely strong and tough hydrogels as prospective candidates for tissue repair–A review, Eur. Polym. J. 72 (2015) 344–364.
[9] A.M.S. Costa, J.F. Mano, Highly robust hydrogels via a fast, simple and cytocompatible dual crosslinking-based process, Chem. Commun. 51 (2015) 15673–15676, https://doi.org/10.1039/C5CC05564D.
[10] J.p. Gong, Y. Katsuyama, T. Kurokawa, Y. Osada, Double-network hydrogels with extremely high mechanical strength, Adv. Mater. 15 (2003) 1155–1158, https://doi.org/10.1002/adma.200304907.
[11] A. Nakayama, A. Kakugo, J.P. Gong, Y. Osada, M. Takai, T. Erata, S. Kawano, High mechanical strength double-network hydrogel with bacterial cellulose, Adv. Funct. Mater. 14 (2004) 1124–1128, https://doi.org/10.1002/adfm.200305197.
[12] L. Weng, A. Gouldstone, Y. Wu, W. Chen, Mechanically strong double network photocrosslinked hydrogels from N, N-dimethylacrylamide and glycidyl methacrylated hyaluronan, Biomaterials 29 (2008) 2153–2163, https://doi.org/10.1016/j.biomaterials.2008.01.012.
[13] K. Haraguchi, T. Takehisa, Nanocomposite hydrogels: a unique organic–inorganic network structure with extraordinary mechanical, optical, and swelling/de-swelling properties, Adv. Mater. 14 (2002) 1120–1124, https://doi.org/10.1002/1521-4095(20020816)14:16<1120::AID-ADMA1120>3.0.CO;2-9.
[14] A.K. Gaharwar, N.A. Peppas, A. Khademhosseini, Nanocomposite hydrogels for biomedical applications, Biotechnol. Bioeng. 111 (2014) 441–453, https://doi.org/10.1002/bit.25160.
[15] K.J. Henderson, T.C. Zhou, K.J. Otim, K.R. Shull, Ionically cross-linked triblock copolymer hydrogels with high strength, Macromolecules 43 (2010) 6193–6201, https://doi.org/10.1021/ma100963m.
[16] K.H. Bouhadir, D.S. Hausman, D.J. Mooney, Synthesis of cross-linked poly(aldehyde guluronate) hydrogels, Polymer 40 (1999) 3575–3584, https://doi.org/10.1016/S0032-3861(98)00550-3.
[17] E.F.S. Vieira, A.R. Cestari, C. Airoldi, W. Loh, Polysaccharide-based hydrogels: preparation, characterization, and drug interaction behaviour, Biomacromolecules 9 (2008) 1195–1199, https://doi.org/10.1021/bm7011983.
[18] M. Prabaharan, J.F. Mano, Stimuli-responsive hydrogels based on polysaccharides incorporated with thermo-responsive polymers as novel biomaterials, Macromol. Biosci. 6 (2006) 991–1008.
[19] E. Boanini, K. Rubini, S. Panzavolta, A. Bigi, Chemico-physical characterization of gelatin films modified with oxidized alginate, Acta Biomater. 6 (2010) 383–388, https://doi.org/10.1016/j.actbio.2009.06.015.
[20] C.L. Bayer, É.P. Herrero, N.A. Peppas, Alginate films as macromolecular imprinted matrices, J. Biomater. Sci. Polym. Ed. 22 (2011) 1523–1534, https://doi.org/10.1163/092050610X514115.
[21] N. Faramarzi, I.K. Yazdi, M. Nabavinia, A. Gemma, A. Fanelli, A. Caizzone, L.M. Ptaszek, I. Sinha, A. Khademhosseini, J.N. Ruskin, A. Tamayol, Patient-specific bioinks for 3D bioprinting of tissue engineering scaffolds, Adv. Healthcare Mater. 7 (2018), 1701347, https://doi.org/10.1002/adhm.201701347.
[22] A. Tamayol, A.H. Najafabadi, B. Aliakbarian, E. Arab-Tehrany, M. Akbari, N. Annabi, D. Juncker, A. Khademhosseini, Hydrogel templates for rapid manufacturing of bioactive fibers and 3D constructs, Adv. Healthcare Mater. 4 (2015) 2146–2153, https://doi.org/10.1002/adhm.201500492.
[23] M. Comotto, S. Saghazadeh, S. Bagherifard, B. Aliakbarian, M. Kazemzadeh-Narbat, F. Sharifi, S.A. Mousavi Shaegh, E. Arab-Tehrany, N. Annabi, P. Perego, A. Khademhosseini, A. Tamayol, Breathable hydrogel dressings containing natural antioxidants for management of skin disorders, J. Biomater. Appl. 33 (2019) 1265–1276, https://doi.org/10.1177/0885328218816526.
[24] A. Duconseille, T. Astruc, N. Quintana, F. Meersman, V. Sante-Lhoutellier, Gelatin structure and composition linked to hard capsule dissolution: a review, Food Hydrocolloids 43 (2015) 360–376, https://doi.org/10.1016/j.foodhyd.2014.06.006.
[25] X. Li, J. Zhang, N. Kawazoe, G. Chen, Fabrication of highly crosslinked gelatin hydrogel and its influence on chondrocyte proliferation and phenotype, Polymers 9 (2017) 309, https://doi.org/10.3390/polym9080309.
[26] M. De, P.S. Ghosh, V.M. Rotello, Applications of nanoparticles in biology, Adv. Mater. 20 (2008) 4225–4241, https://doi.org/10.1002/adma.200703183.
[27] Nanoparticles: Properties, Classification, Characterization, and Fabrication by Aiden E. Kestell, Gabriel T. DeLorey: Nova Science Publishers Inc 9781616683443 Hardback - THE SAINT BOOKSTORE, (n.d.). http://www.abebooks.com/servlet/BookDetailsPL?bi=5962576156&searchurl=sortby=20&an=aiden%20e%20kestell%20gabriel%20t%20delorey (accessed October 23, 2015).
[28] V. Rotello, Nanoparticles: Building Blocks for Nanotechnology, Springer Science & Business Media, 2012.
[29] S. Pina, J.M. Oliveira, R.L. Reis, Natural-based nanocomposites for bone tissue engineering and regenerative medicine: a review, Adv. Mater. 27 (2015) 1143–1169, https://doi.org/10.1002/adma.201403354.
[30] D.A. Tomalia, In quest of a systematic framework for unifying and defining nanoscience, J. Nanoparticle Res. 11 (2009) 1251–1310, https://doi.org/10.1007/s11051-009-9632-z.
[31] S.-I. Roohani-Esfahani, H. Zreiqat, Nanoparticles: a promising new therapeutic platform for bone regeneration? Nanomedicine 12 (2017) 419–422, https://doi.org/10.2217/nnm-2016-0423.
[32] M. Linder, E. Matouba, J. Fanni, M. Parmentier, Enrichment of salmon oil with n-3 PUFA by lipolysis, filtration and enzymatic re-esterification, Eur. J. Lipid Sci. Technol. 104 (2002) 455–462.
[33] R.G. Ackman, Remarks on official methods employing boron trifluoride in the preparation of methyl esters of the fatty acids of fish oils, J. Am. Oil Chem. Soc. 75 (1998) 541–545, https://doi.org/10.1007/s11746-998-0263-9.
[34] E.K. Dimitriadis, F. Horkay, J. Maresca, B. Kachar, R.S. Chadwick, Determination of elastic moduli of thin layers of soft material using the atomic force microscope, Biophys. J. 82 (2002) 2798–2810, https://doi.org/10.1016/S0006-3495(02)75620-8.
[35] P. Polyakov, C. Soussen, J. Duan, J.F.L. Duval, D. Brie, G. Francius, Automated force volume image processing for biological samples, PloS One 6 (2011), https://doi.org/10.1371/journal.pone.0018887 e18887.
[36] J. Dupont, P.J. White, K.M. Johnston, H.A. Heggtveit, B.E. McDonald, S.M. Grundy, A. Bonanome, Food safety and health effects of canola oil, J. Am. Coll. Nutr. 8 (1989) 360–375, https://doi.org/10.1080/07315724.1989.10720311.
[37] D. Coonrod, M.A. Brick, P.F. Byrne, L. DeBonte, Z. Chen, Inheritance of long chain fatty acid content in rapeseed (Brassica napus L.), Euphytica 164 (2008) 583–592, https://doi.org/10.1007/s10681-008-9781-7.
[38] Pharmaceutical Press - Handbook of Pharmaceutical Excipients Seventh Edition, (n.d.). http://www.pharmpress.com/product/9780857110275/excipients (accessed October 23, 2015).
[39] A.R.C. Duarte, J.F. Mano, R.L. Reis, Preparation of chitosan scaffolds loaded with dexamethasone for tissue engineering applications using supercritical fluid technology, Eur. Polym. J. 45 (2009) 141–148, https://doi.org/10.1016/j.eurpolymj.2008.10.004.
[40] Y.S. Tarahovsky, E.A. Yagolnik, E.N. Muzafarov, B.S. Abdrasilov, Y.A. Kim, Calcium-dependent aggregation and fusion of phosphatidylcholine liposomes induced by complexes of flavonoids with divalent iron, Biochim. Biophys. Acta 1818 (2012) 695–702, https://doi.org/10.1016/j.bbamem.2011.12.001.
[41] Y. Liu, Z. Li, D. Liang, Behaviors of liposomes in a thermo-responsive poly(N-isopropylacrylamide) hydrogel, Soft Matter 8 (2012) 4517–4523, https://doi.org/10.1039/C2SM25092F.
[42] J.C. Stendahl, M.S. Rao, M.O. Guler, S.I. Stupp, Intermolecular forces in the self-assembly of peptide amphiphile nanofibers, Adv. Funct. Mater. 16 (2006) 499–508, https://doi.org/10.1002/adfm.200500161.
[43] G. Ben Messaoud, L. Sánchez-González, L. Probst, S. Desobry, Influence of internal composition on physicochemical properties of alginate aqueous-core capsules, J. Colloid Interface Sci. 469 (2016) 120–128, https://doi.org/10.1016/j.jcis.2016.02.018.
[44] G.T. Grant, E.R. Morris, D.A. Rees, P.J.C. Smith, D. Thom, Biological interactions between polysaccharides and divalent cations: the egg-box model, FEBS (Fed. Eur. Biochem. Soc.) Lett. 32 (1973) 195–198, https://doi.org/10.1016/0014-5793(73)80770-7.

[45] D. Papahadjopoulos, S. Nir, N. Düzgünes, Molecular mechanisms of calcium-induced membrane fusion, J. Bioenerg. Biomembr. 22 (1990) 157–179, https://doi.org/10.1007/BF00762944.
[46] A.I. Van Den Bulcke, B. Bogdanov, N. De Rooze, E.H. Schacht, M. Cornelissen, H. Berghmans, Structural and rheological properties of methacrylamide modified gelatin hydrogels, Biomacromolecules 1 (2000) 31–38, https://doi.org/10.1021/bm990017d.
[47] C. Joly-Duhamel, D. Hellio, A. Ajdari, M. Djabourov, All gelatin Networks: 2. The master curve for elasticity, Langmuir 18 (2002) 7158–7166, https://doi.org/10.1021/la020190m.
[48] S.K. Samal, M. Dash, S.V. Vlierberghe, D.L. Kaplan, E. Chiellini, C. van Blitterswijk, L. Moroni, P. Dubruel, Cationic polymers and their therapeutic potential, Chem. Soc. Rev. 41 (2012) 7147–7194, https://doi.org/10.1039/C2CS35094G.